J. Meas. Sci. Instrum., 2025, 16(3): 384-394. http://jmsi.publish.founderss.cn
DOI: 10.62756/jmsi.1674-8042.2025037 jmsi@nuc.edu.cn

Improved Gabor transform and group sparse representation for ancient mural inpainting

ZHAO Mengxue[1], CHEN Yong[1,2*], TAO Meifeng[1]

1. School of Electronic Engineering, Lanzhou Jiaotong University, Lanzhou 730070, China;
2. Gansu Provincial Engineering Research Center for Artificial Intelligence and Graphics & Image Processing, Lanzhou 730070, China

***Corresponding author:** CHEN Yong (edukeylab@126.com)

Received: January 3, 2024 **Revised:** January 18, 2024 **Accepted:** January 24, 2024

Abstract: Sparse representation has been highly successful in various tasks related to image processing and computer vision. For ancient mural image inpainting, traditional group sparse representation models usually lead to structure blur and line discontinuity due to the construction of similarity group solely based on the Euclidean distance and the randomness of dictionary initialization. To address the aforementioned issues, an improved curvature Gabor transform and group sparse representation (CGabor-GSR) model for ancient Dunhuang mural inpainting is proposed. To begin with, mutual information is introduced to weight the Euclidean distance, and then the weighted Euclidean distance acts as a new standard of similarity group. Subsequently, to mitigate the randomness of dictionary initialization, a curvature Gabor wavelet transform is proposed to extract the features and initialize the feature dictionary with dimension reduction based on principal component analysis (PCA). Ultimately, singular value decomposition (SVD) and split Bregman iteration (SBI) can be used to resolve the CGabor-GSR model to reconstruct the mural images. Experimental results on Dunhuang mural inpainting demonstrate tha the proposed CGabor-GSR achieves a better performance than compared algorithms in both objective and visual evaluation.

Key words: digital image processing; mural inpainting; curvature Gabor wavelet transform; group sparse representation; mutual information

0 Introduction

The murals in the Dunhuang Mogao Grottoes are typical representatives of artistic and cultural heritage, which show the color painting techniques of ancient Chinese artists spanning the 4th to the 14th centuries, and have high artistic research value and archaeological value. Centuries of exposure to harsh environmental conditions have induced progressive deterioration in murals, and corrosion and aging problems urgently need to be addressed, including mold, cracks, smoke, and large-scale peeling. In the process of repairing damaged murals, manual restoration relying solely on painting experience may easily give rise to restorative damage such as color differences and comprehension errors. Therefore, the usage of digital image processing technology for automatic restoration of ancient murals via data-driven methods has become a research hotspot in the field of image processing.

Traditional inpainting methods can usually be divided into geometry based repair methods[1-6] and sparse representation based repair methods[7-10]. Among them, geometry based repair methods include pixel diffusion based energy equation method[1,2], and sample matching method based on similar block texture synthesis[3-6]. The former performs diffusion repair by transitioning edge prior pixels towards the missing center, but it is applicable to only small damaged areas such as cracks. For the situations with complex structures and large defects, incomplete repair and over smoothing may occur. The main repair algorithms include Bertalmio Sapiro Caselles Bellester (BSCB) model, total variation (TV), and curvature driven diffusion (CDD)[11-13]. The latter guides the repair order by defining block priority, copies the information of source area sample blocks to the corresponding target area, and determines the priority of the isolines. It prioritizes the propagation of known parts at the boundary between textures into the area to be repaired, completing the repair. This method can repair large damaged images, but has problems of incorrect sample block matching and structural

© The Author(s) 2025. Published by Publishing Center of North University of China. The articles published in this open access journal are distributed under the terms of the Creative Commons Attribution 4.0 International License (http://creativecommons.org/licenses/by/4.0/), which permits use, distribution and reproduction in any medium, provided the original work is properly cited.

distortion caused by improper repair sequence[14,15], represented by the Criminisi algorithm[16].

The sparse representation based repair algorithm calculates the sparse encoding of damaged blocks on an overcomplete dictionary, thereby transforming dense samples into sparse expressions and reconstructing damaged areas using sparse encoding and overcomplete dictionaries. The training dictionary for sparse models can be divided into fixed base dictionaries with low computational cost but poor adaptive ability[17,18] and learning dictionaries with high flexibility and fast convergence speed[19]. Qin[20] proposed a sparse representation method using a model-based pulse wavelet dictionary, and sparsely represented it using pulse wavelet basis. Zhang et al.[21] proposed a group sparse representation (GSR) algorithm considering the similarity between image blocks. However, this method only groups similar image blocks based on the Euclidean distance, resulting in discontinuous lines and poor texture clarity when repairing complex mural images. Zha et al.[22] proposed a method of joint patch-group based sparse representation (JPG-SR) for image repair, but it applies K-singular value decomposition (K-SVD) dictionary and grouped sparse principal component analysis (PCA) dictionary to image patches for combination of block groups, and utilizes alternating direction method of multipliers (ADMM) for iterative solution, resulting in high computational complexity. Kong et al. [23] proposed a group sparse representation model based on multiple color channels, which simultaneously processes three primary color channels and combines the repair results of each channel in the repaired image. Since it does not simultaneously consider the texture structure features of the image, texture blurs occur. Wang et al.[24] completed the filling of damaged areas by linearly weighting global and local features. However, this method obtains global and local features by constructing a sparse repair model and estimating domain similar features respectively, algorithmic complexity becomes high.

In summary, in response to the problems of structural ambiguity and discontinuous lines caused by traditional group sparse representation models using the Euclidean distance to construct similar groups, we propose a model for mural inpainting based on curvature Gabor transform and group sparse representation (CGabor-GSR).

The main contributions of this study are as follows:

1) To overcome the drawback of constructing similarity groups solely based on the Euclidean distance, we weight the Euclidean distance by introducing mutual information, and then use the weighted Euclidean distance to partition similar groups, thus taking full advantage of the image features when computing the similarity between sample blocks and matching blocks.

2) Due to the random initialization of dictionary, it is easy to fall into local optimum, which leads to blurred structure and incoherent lines. To solve this problem, we propose a curvature Gabor (CGabor) wavelet transform to extract the features of structure groups, and initiate the feature dictionary of the structure groups with PCA dimension reduction.

3) The CGabor-GSR can be solved by using SVD and split Bregman iteration (SBI) optimization algorithm to reconstruct the damaged mural images.

1 Sparse representation model

Sparse representation, also known as sparse coding, is to express a given signal using as few atoms as possible in a linear combination from an overcomplete dictionary, thereby simplifying the expression of the signal[25]. Since the dictionary $\boldsymbol{D}$ is overcomplete and full-rank, the essence of sparse representation is to find the best sparse coefficient $\boldsymbol{\alpha}$ that satisfies sparsity and guarantees the reconstruction of signal $\boldsymbol{S}$ within the given dictionary $\boldsymbol{D}$.

The mathematical definition of optimization problem is

$$\begin{aligned} &\arg\min_{\alpha} \|\boldsymbol{\alpha}\|_0, \\ &\text{s.t. } \boldsymbol{S}=\boldsymbol{D}\boldsymbol{\alpha}, \end{aligned} \tag{1}$$

where $\|\boldsymbol{\alpha}\|_0$ is the l_0-norm, standing for the number of non-zero elements in the vector to measure the sparsity of the coefficient.

Donoho[26] and Candes et al.[27] have proven that under the condition of signal sparsity, the convex optimization approximation problem can be solved using l_1-norm instead of l_0-norm as

$$\arg\min_{\alpha} \|\boldsymbol{\alpha}\|_1, \quad \text{s.t. } \boldsymbol{S}=\boldsymbol{D}\boldsymbol{\alpha}. \tag{2}$$

Generally, natural images tend to corrupt by noise or have certain reconstruction error ε. When the parameter λ is used to balance the sparsity and reconstruction errors, Eq. (2) can be rewritten as

$$\begin{aligned} &\arg\min_{\alpha} \frac{1}{2}\|\boldsymbol{S}-\boldsymbol{D}\boldsymbol{\alpha}\|_2+\lambda\|\boldsymbol{\alpha}\|_1, \\ &\text{s.t. } \|\boldsymbol{S}-\boldsymbol{D}\boldsymbol{\alpha}\|_2 \leqslant \varepsilon. \end{aligned} \tag{3}$$

Image inpainting is the inverse problem of using the prior information of image to reconstruct degraded image. Assuming that an original mural image $\boldsymbol{X}$ is degraded by a noninvertible linear operator $\boldsymbol{J}$ and an additive Gaussian white noise $\boldsymbol{n}$, for certain image inpainting problems[28], the observed image $\boldsymbol{Y}$ can be mathematically modeled by

$$\boldsymbol{Y}=\boldsymbol{JX}+\boldsymbol{n}. \tag{4}$$

From Eq. (3), in the case of a given dictionary, the image inpainting process can be transformed into a problem of solving the sparse coefficient $\boldsymbol{\alpha}$, and the mathematical definition is

$$\boldsymbol{\alpha}=\arg\min_{\alpha}\frac{1}{2}\|\boldsymbol{Y}-\boldsymbol{JD\alpha}\|_2+\lambda\|\boldsymbol{\alpha}\|_1. \tag{5}$$

After obtaining the sparsity coefficient, the image can be reconstructed.

2 Proposed model

2.1 Group construction based on weighted mutual information

In information theory, mutual information measures the correlation between sample features and categories based on the probability of co-occurrence of them. The greater the mutual information, the higher the degree of correlation between categories. We introduce the mutual information to weight the Euclidean distance as a standard to measure the similarity of image blocks and construct the structure group. The mutual information between image blocks is calculated by

$$I(\boldsymbol{A},\boldsymbol{B}_j)=H(\boldsymbol{A})+H(\boldsymbol{B}_j)-H(\boldsymbol{A},\boldsymbol{B}_j), \tag{6}$$

where $H(\boldsymbol{A})$ is the information entropy of sample block $\boldsymbol{A}$; $H(\boldsymbol{B}_j)$ is the information entropy of the jth matching block $\boldsymbol{B}_j$; and $H(\boldsymbol{A},\boldsymbol{B}_j)$ is the joint entropy between the sample block $\boldsymbol{A}$ and the matching block $\boldsymbol{B}_j$. The information entropy and joint entropy of the image block are respectively calculated by

$$H(\boldsymbol{A})=-\sum_{i=0}^{255}P_A(i)\log_2\left[P_A(i)\right]/3, \tag{7}$$

$$H(\boldsymbol{B}_j)=-\sum_{i=0}^{255}P_{B_j}(i)\log_2\left[P_{B_j}(i)\right]/3, \tag{8}$$

$$H(\boldsymbol{A},\boldsymbol{B}_j)=-\sum_{i=0}^{255}P_{AB_j}(i)\log_2\left[P_{AB_j}(i)\right]/3, \tag{9}$$

where $P_A(i)$ and $P_{B_j}(i)$ are the ratios of pixels at the ith level of the three RGB color channels in image blocks $\boldsymbol{A}$ and $\boldsymbol{B}_j$, respectively; $P_{AB_j}(i)$ is the joint proportion of pixels at the ith level of image blocks $\boldsymbol{A}$ and $\boldsymbol{B}_j$; and i represents the pixel level, with values from 0 to 255. Thus, the weight is calculated by

$$w_j=\frac{I(\boldsymbol{A},\boldsymbol{B}_j)}{\sum_{j=1}^{c}I(\boldsymbol{A},\boldsymbol{B}_j)}, \tag{10}$$

where c is the number of matching blocks, and w_j is the weight of the jth matching block, satisfying $\sum_{j=1}^{c}w_j=1$.

The weighted Euclidean distance between sample block $\boldsymbol{A}$ and the jth matching block $\boldsymbol{B}_j$ is calculated by

$$d(\boldsymbol{A},\boldsymbol{B}_j)=\sqrt{w_j(\boldsymbol{A}-\boldsymbol{B}_j)^2}. \tag{11}$$

According to the weighted Euclidean distance, the similarity between sample blocks and matching blocks is calculated, which not only utilizes the features of the image well, but also avoids insufficiently considering signal source attributes when segmenting image blocks only by the Euclidean distance.

The construction of a group can be divided into three stages: extracting, matching and stacking, as shown in Fig.1.

1) Dividing the mural image $\boldsymbol{X}$ into patches, each with a size of $\sqrt{B_s}\times\sqrt{B_s}$, and extracting the sample patch $\boldsymbol{X}_k\in\mathrm{R}^{B_s}$.

2) For each patch $\boldsymbol{X}_k$, in the $L\times L$ searching windows, the weighted Euclidean distance is calculated as the similarity criterion between different patches and its c best matched patches are searched to comprise the set S_{X_k}.

3) All the patches in S_{X_k} are stacked into a matrix with a size of $B_s\times c$, which contains every patch in S_{X_k}, that is, $\boldsymbol{X}_{G_k}\in\{\boldsymbol{X}_{G_k\otimes 1},\boldsymbol{X}_{G_k\otimes 2},\cdots,\boldsymbol{X}_{G_k\otimes c}\}$, where $\boldsymbol{X}_{G_k}$ containing all the patches with similar structure is referred to as a structure group.

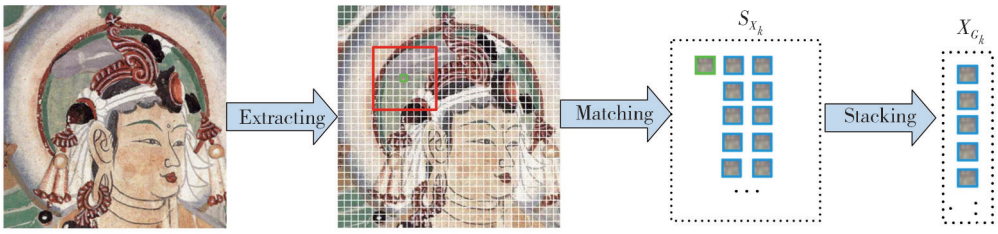

Fig. 1 Construction of structure group

We define

$$\boldsymbol{X}_{G_k}=\boldsymbol{R}_{G_k}(\boldsymbol{X}), \tag{12}$$

where $\boldsymbol{R}_{G_k}(\cdot)$ is actually an operator that extracts the group $\boldsymbol{X}_{G_k}$ from $\boldsymbol{X}$, and its transpose is denoted by $\boldsymbol{R}_{G_k}^{\mathrm{T}}(\cdot)$, which puts back a group into the kth position in the reconstructed image, padded with zeros elsewhere.

By averaging all the groups, the inpainting of the whole image $\boldsymbol{X}$ from $\boldsymbol{X}_{G_k}$ becomes

$$\boldsymbol{X}=\sum_{k=1}^{n}\boldsymbol{R}_{G_k}^{\mathrm{T}}(\boldsymbol{X}_{G_k})./\sum_{k=1}^{n}\boldsymbol{R}_{G_k}^{\mathrm{T}}(\boldsymbol{1}_{B_k\times c}), \tag{13}$$

where ./ stands for the element-wise division of two vectors, and $\boldsymbol{1}_{B_k\times c}$ is a matrix with a size of $B_k\times c$ and all the elements being 1.

$$\boldsymbol{\alpha}_{G_k}=\arg\min_{\boldsymbol{\alpha}_{G_k}}\frac{1}{2}\left\|\boldsymbol{X}_{G_k}-\boldsymbol{D}_{G_k}\boldsymbol{\alpha}_{G_k}\right\|_2^2+\lambda\left\|\boldsymbol{\alpha}_{G_k}\right\|_1. \tag{14}$$

As shown in Eq. (14), the core of sparse representation model lies in the initialization of dictionary $\boldsymbol{D}$, which plays a crucial role in the image inpainting process and determines the solution quality of the image inverse problem[29]. If the dictionary is initialized by randomly selected samples, the learning of the dictionary may easily fall into local optimum, resulting in poor image inpainting effects. Therefore, to overcome the blindness of initial dictionary construction and extract the feature information of murals well, we propose to use curvature Gabor wavelet transform to extract the features of similar structure groups $\boldsymbol{X}_{G_k}$, and perform PCA dimensionality reduction on high-dimensional features to obtain the feature dictionary within the group $\boldsymbol{D}_{G_k}$.

2.2 Curvature Gabor-PCA dictionary

The traditional Gabor filters[30,31] perform multi-scale and multi-directional feature extraction on the image, without considering the curvature information of images. To solve this problem, we propose a CGabor filter to extract more abundant information, which has good curvature effect and stronger robustness.

The Gabor wavelet transform of the image is to convolve the image with the Gabor kernel function. Based on the constructed structure group $\boldsymbol{X}_{G_k}$, the kernel function of the Gabor filter is defined as

$$G(x,y)=\frac{1}{2\pi\sigma^2}\exp\left(-\frac{x^2+y^2}{2\sigma^2}\right)\exp\left[2\pi\mathrm{i}(ux'+uy')\right], \tag{15}$$

where x' and y' are defined as

$$\begin{cases}x'=x\cos\theta+y\sin\theta,\\ y'=y\cos\theta-x\sin\theta.\end{cases} \tag{16}$$

Then, Eq. (15) is transformed into

$$G(x,y)=\frac{1}{2\pi\sigma^2}\exp\left(-\frac{x^2+y^2}{2\sigma^2}\right)\exp\left[2\pi\mathrm{i}(ux\cos\theta+uy\sin\theta)\right], \tag{17}$$

where (x,y) is the pixel coordinates of the structure group $\boldsymbol{X}_{G_k}$; θ is the direction angle of the sine wave; u is approximately defined as $u=\frac{1}{\sigma}$; and σ is the standard deviation of the Gaussian function, reflecting the scale characteristics of the filter.

Then, each image block in the structure group image is convolved with Gabor kernel function to extract Gabor features, and the mathematical definition is

$$O_{u,v}(x,y)=X_{G_k}(x,y)*G(x,y), \tag{18}$$

where * is the convolution operation, $X_{G_k}(x,y)$ is the pixel coordinates of the structure group, $G(x,y)$ is the Gabor kernel function, and $O_{u,v}(x,y)$ is the Gabor feature maps at different scales and directions.

The Gabor filter is used to extract the features from the image blocks of the mural image as an example. Fig. 2 shows the features extracted by the Gabor filter through five scales and eight directions. It can be seen that the structure of feature mapping and texture details are blurred.

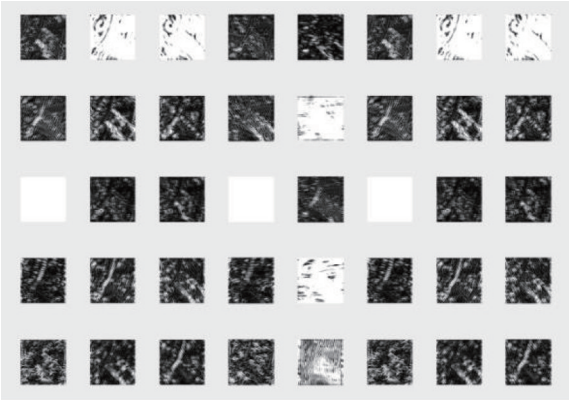

Fig. 2 Image blocks after feature extraction by Gabor filter

The images of Dunhuang murals are composed of a large number of curves. From a biological point of view, the cerebral cortex has a strong stimulus response to the curled image components. Based on this, we introduce curvature into the Gabor filter. Therefore, while maintaining the multi-scale and multi-direction of the Gabor filter, the curvature of the image is utilized to further improve the feature extraction performance.

Based on the traditional filter, the coordinates are improved as

$$\begin{cases}x'=x\cos\theta+y\sin\theta+t(y\cos\theta-x\sin\theta)^2,\\ y'=y\cos\theta-x\sin\theta,\end{cases} \tag{19}$$

where t is a parameter that represents the curvature of the local area of the image. The multiple sets of experiments show that the filtering effect is better when t is 0.1.

To further explain the effect of CGabor filter, a comparison between the traditional Gabor filter and the CGabor filter is made, and the results are shown in Fig. 3. It can be observed that the traditional Gabor filter does not take into account the degree of curvature of the image lines, while the CGabor filter has good curvature

response characteristics to the local bending areas, which means its filtering performance is better.

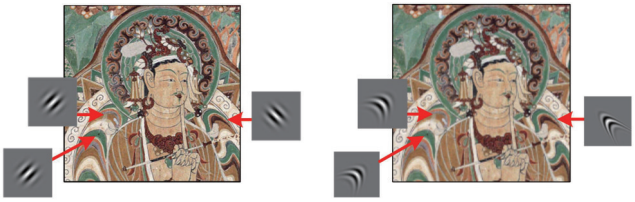

(a) Traditional Gabor filter (b) CGabor filter

Fig. 3 Comparison of traditional Gabor filter and urvature CGabor filter

To verify the effectiveness of the proposed CGabor filter, experiments were conducted on the same image blocks shown in Fig.2, and experimental results are shown in Fig.4. Compared to the results by the traditional filter, the filtered images by the CGabor filter have richer structural and textural information, and the curvature responses are better in curved regions of the image.

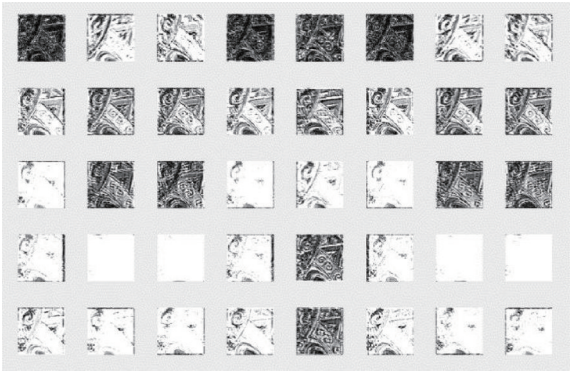

Fig. 4 Image blocks after feature extraction by CGabor filter

To achieve lossless representation of images, Gabor transform requires eight discrete equidistant directions and five equidistant scales at each discrete position[32], thereby producing a 40-dimensional feature dictionary. Since some feature maps of the dictionary have redundancy or less feature information, it is necessary to reduce the dimensionality of the feature maps. Therein, we adopt PCA dimensionality reduction method to obtain the initial feature dictionary $\boldsymbol{D}_{G_k}$ of each structure group $\boldsymbol{X}_{G_k}$.

When performing PCA dimensionality reduction, first, the feature map of each structure group $\boldsymbol{X}_{G_k}$ is expressed in the form of a vector, that is, $\boldsymbol{H}=\left[\boldsymbol{h}_1,\boldsymbol{h}_2,\cdots,\boldsymbol{h}_l,\cdots,\boldsymbol{h}_M\right]^{\mathrm{T}}$, which is subsequently arranged in rows to form a P-dimensional column vector, finally obtaining a $P\times M$ dimensional matrix. Thus, the average vector of the feature map in each structure group is calculated by

$$\boldsymbol{\psi}_{G_k}=\frac{1}{M}\sum_{i=1}^{M}\boldsymbol{h}_i, \tag{20}$$

where $\boldsymbol{h}_l$ stands for the Gabor feature map, and M is the total number of feature maps in each structure group.

Next, by performing the deviation of the average column vectors from the column vectors of the feature map, the feature map is decentralized. The calculation of covariance between subsequent features is simplified as

$$\boldsymbol{A}_{G_k}=\left[\boldsymbol{h}_1-\boldsymbol{\psi}_{G_k},\boldsymbol{h}_2-\boldsymbol{\psi}_{G_k},\cdots,\boldsymbol{h}_M-\boldsymbol{\psi}_{G_k}\right]=\left[\boldsymbol{\xi}_1,\boldsymbol{\xi}_2,\cdots,\boldsymbol{\xi}_P,\cdots,\boldsymbol{\xi}_M\right]. \tag{21}$$

To de-centralize the eigenvalue column vectors, the covariance matrix is further calculated by

$$\boldsymbol{C}_{G_k}=\frac{1}{M}\sum_{P=1}^{M}\boldsymbol{\xi}_P\boldsymbol{\xi}_P^{\mathrm{T}}=\frac{1}{M}\boldsymbol{A}_{G_k}\boldsymbol{A}_{G_k}^{\mathrm{T}}. \tag{22}$$

Finally, after calculating the feature vectors of $\boldsymbol{A}_{G_k}\boldsymbol{A}_{G_k}^{\mathrm{T}}$, it is arranged according to the size of the corresponding feature value, thus reducing the dimensionality and obtaining the feature subspace. When projecting the feature maps onto the feature subspace, we obtain the feature dictionary within the structure group $\boldsymbol{D}_{G_k}$ via PCA dimensiona reduction.

2.3 Dictionary learning and sparse coding

In this section, we will show how to adopt SVD and SBI [33-35] to learn the adaptive dictionary $\boldsymbol{D}_{G_k}$ and solve the sparse coefficient $\boldsymbol{\alpha}_{G_k}$ for each group $\boldsymbol{X}_{G_k}$.

First, the bilinear interpolation algorithm is used to obtain the estimated value $\boldsymbol{r}_{G_k}$ of the structure group $\boldsymbol{X}_{G_k}$, and then we apply SVD to it, that is,

$$\boldsymbol{r}_{G_k}=\boldsymbol{U}_{G_k}\boldsymbol{\Sigma}_{G_k}\boldsymbol{V}_{G_k}^{\mathrm{T}}=\sum_{i=1}^{m}\boldsymbol{r}_{G_k\otimes i}(\boldsymbol{u}_{G_k\otimes i}\boldsymbol{v}_{G_k\otimes i}^{\mathrm{T}}), \tag{23}$$

where $\boldsymbol{U}_{G_k}$ and $\boldsymbol{V}_{G_k}$ are the left and right singular orthogonal matrices of the structure group $\boldsymbol{X}_{G_k}$, respectively; $\boldsymbol{\Sigma}_{G_k}$ is a diagonal matrix with the elements of $\boldsymbol{r}_{G_k\otimes i}$ on its main diagonal; and $\boldsymbol{u}_{G_k\otimes i}$ and $\boldsymbol{v}_{G_k\otimes i}$ are the columns of $\boldsymbol{U}_{G_k}$ and $\boldsymbol{V}_{G_k}$, respectively. Each atom in $\boldsymbol{D}_{G_k}$ for group $\boldsymbol{X}_{G_k}$ is expressed as

$$\boldsymbol{d}_{G_{k\otimes i}}=\boldsymbol{u}_{G_k\otimes i}\boldsymbol{v}_{G_k\otimes i}^{\mathrm{T}},\ i=1,2,\cdots,k. \tag{24}$$

Therefore, the adaptive dictionary corresponding to structure group is defined as

$$\boldsymbol{D}_{G_k}=\left[\boldsymbol{d}_{G_{k\otimes 1}},\boldsymbol{d}_{G_{k\otimes 2}},\cdots,\boldsymbol{d}_{G_{k\otimes k}}\right]. \tag{25}$$

The advantage of SVD dictionary learning for each group is to ensure that all the patches in each group use the same dictionary and share the same dictionary atoms, which is more effective and robust.

After obtaining $\boldsymbol{D}_{G_k}$ of the structure group, we adopt the framework of SBI to solve the sparse coefficient $\boldsymbol{\alpha}_{G_k}$. By introducing variable β, Eq. (14) is transformed into

an equivalent constraint form as

$$\boldsymbol{\alpha}_{G_k}=\arg\min_{\boldsymbol{\alpha}_{G_k},\beta}\frac{1}{2}\left\|J\beta-Y\right\|_2^2+\lambda\left\|\boldsymbol{\alpha}_{G_k}\right\|_1,$$
$$\text{s.t. }\beta=\boldsymbol{D}_{G_k}\boldsymbol{\alpha}_{G_k}. \tag{26}$$

Finally, image reconstruction is completed with the dictionary $\boldsymbol{D}_{G_k}$ and the sparse coefficient $\boldsymbol{\alpha}_{G_k}$.

The overall algorithm is summarized in Algorithm 1.

Algorithm 1: CGabor-GSR algorithm

Input: An original mural image $\boldsymbol{X}$ and the degraded operator $\boldsymbol{J}$.
Output: The final inpainted image.
1: **Initialization**: $\lambda, c, B_s, L, \beta$
2: **For** $k=1$ to *iterNum* do
3: Calculate weighted Euclidean distance $d(\boldsymbol{A},\boldsymbol{B})=\sqrt{w_j(\boldsymbol{A}-\boldsymbol{B})^2}$
4: Find similar patches to form structure group $\boldsymbol{X}_{G_k}$
5: Initialize dictionary $\boldsymbol{D}_{G_k}$ with curvature Gabor-PCA
6: Update dictionary via SVD:
$$\boldsymbol{r}_{G_k}=\boldsymbol{U}_{G_k}\boldsymbol{\Sigma}_{G_k}\boldsymbol{V}_{G_k}^{\mathrm{T}}=\sum_{i=1}^{m}\boldsymbol{r}_{G_k\otimes i}(\boldsymbol{u}_{G_k\otimes i}\boldsymbol{v}_{G_k\otimes i}^{\mathrm{T}})$$
7: Solve sparse coefficients by SBI:
$$\boldsymbol{\alpha}_{G_k}=\arg\min_{\boldsymbol{\alpha}_{G_k},\beta}\frac{1}{2}\left\|J\beta-Y\right\|_2^2+\lambda\left\|\boldsymbol{\alpha}_{G_k}\right\|_1$$
$$\text{s.t. }\beta=\boldsymbol{D}_{G_k}\boldsymbol{\alpha}_{G_k}$$
8: Update image:
$$\boldsymbol{X}=\boldsymbol{D}\boldsymbol{\alpha}=\textstyle\sum_{k=1}^{n}\boldsymbol{R}_{G_k}^{\mathrm{T}}(\boldsymbol{D}_{G_k}\boldsymbol{\alpha}_{G_k})./\sum_{k=1}^{n}\boldsymbol{R}_{G_k}^{\mathrm{T}}(1_{B_k\times c})$$
9: Iterative regularization
10: $k=k+1$
11: **End for**

3 Experiments and analysis

In this section, to demonstrate the performance of our method, the experiments were carried out under Windows 10 and Matlab R2016a systems, running on a laptop with an Inter(R) Core i7-9700K CPU@3.6GHz, 16.0GB RAM, NVIDIA GeForce GTX 1660.

To quantify the inpainting results, we use the peak signal-to-noise ratio (PSNR) and structural similarity index measurement (SSIM) for performance comparison, and the same variable method to ensure the rigor of the experimental results. The size of each patch is set as 8×8, each structure group contains 60 blocks, and the size of the searching window is 40×40. Experiments were carried out for the damaged images with randomly missing pixels, artificially induced damaged images, and really damaged mural images.

3.1 Damaged images with randomly missing pixels

To validate the effectiveness of the CGabor-GSR, we first conducted a restoration experiment on Dunhuang murals with randomly missing pixels and compared it with representative methods including CDD[13], GSR[21], and JPG-SR[22]. The damaged image with randomly missing pixels is obtained via the binary mask which has only 40% pixels, that is to say, 60% pixels are randomly discarded. The experimental results are shown in Fig. 5. Fig. 5(a) is the original Dunhuang mural image, and Fig. 5(b) is the observed image with 60% pixels missing. The inpainting results of CDD, GSR, JPG-SR and CGabor-GSR are presented in Fig. 5(c) — (f), respectively. Visually, we can easily observe that the inpainting results of CGabor-GSR are much clearer than that of CDD. The CDD is a thermal diffusion image inpainting model, using the gradient and curvature information of the image for diffusion of the pixels to complete the inpainting. However, due to intensive and obvious repair traces on the damaged area will be left, for example, the overall image is blurred and the contour edge information is seriously lost in Fig. 5(c). GSR and JPG-SR have more robust repair effects on mural images with randomly missing pixels, but the repair effect of CGabor-GSR is clearer than that of GSR and JPG-SR, such as the eyes and mouths of mural images in Fig. 5(f).

To further illustrate the effectiveness of the CGabor-GSR, PSNR and SSIM are used for objectively quantitative comparison. Table 1 shows the quantitative comparison results of the PSNR and SSIM values of the four different algorithms in the mural restoration experiment in Fig. 5. It can be concluded that CGabor-GSR is superior to three comparison algorithms of CDD, GSR, and JPG-SR in terms of PSNR and SSIM. The results demonstrate that CGabor-GSR exhibits outstanding performance in inpainting mural images with randomly missing pixels, and the inpainted images have minimal distortion.

Table 1 Comparison of PSNR and SSIM values of four algorithms when inpainting the images with randomly missing pixels

Image No.	CDD		GSR		JPG-SR		CGabor-GSR	
	PSNR /dB	SSIM	PSNR /dB	SSIM	PSNR /dB	SSIM	PSNR /dB	SSIM
1	19.542 3	0.715 3	22.526 4	0.805 1	23.129 4	0.809 4	**24.398 9**	**0.868 7**
2	21.024 6	0.769 8	25.529 1	0.837 2	25.817 7	0.831 1	**26.832 6**	**0.875 1**
3	22.328 2	0.800 1	28.175 8	0.893 4	28.232 5	0.879 2	**30.254 9**	**0.928 4**
4	26.510 5	0.923 1	34.571 5	0.957 8	27.018 5	0.828 6	**37.175 4**	**0.975 7**
5	22.419 4	0.792 6	27.187 4	0.868 8	27.231 7	0.851 8	**29.151 3**	**0.912 2**

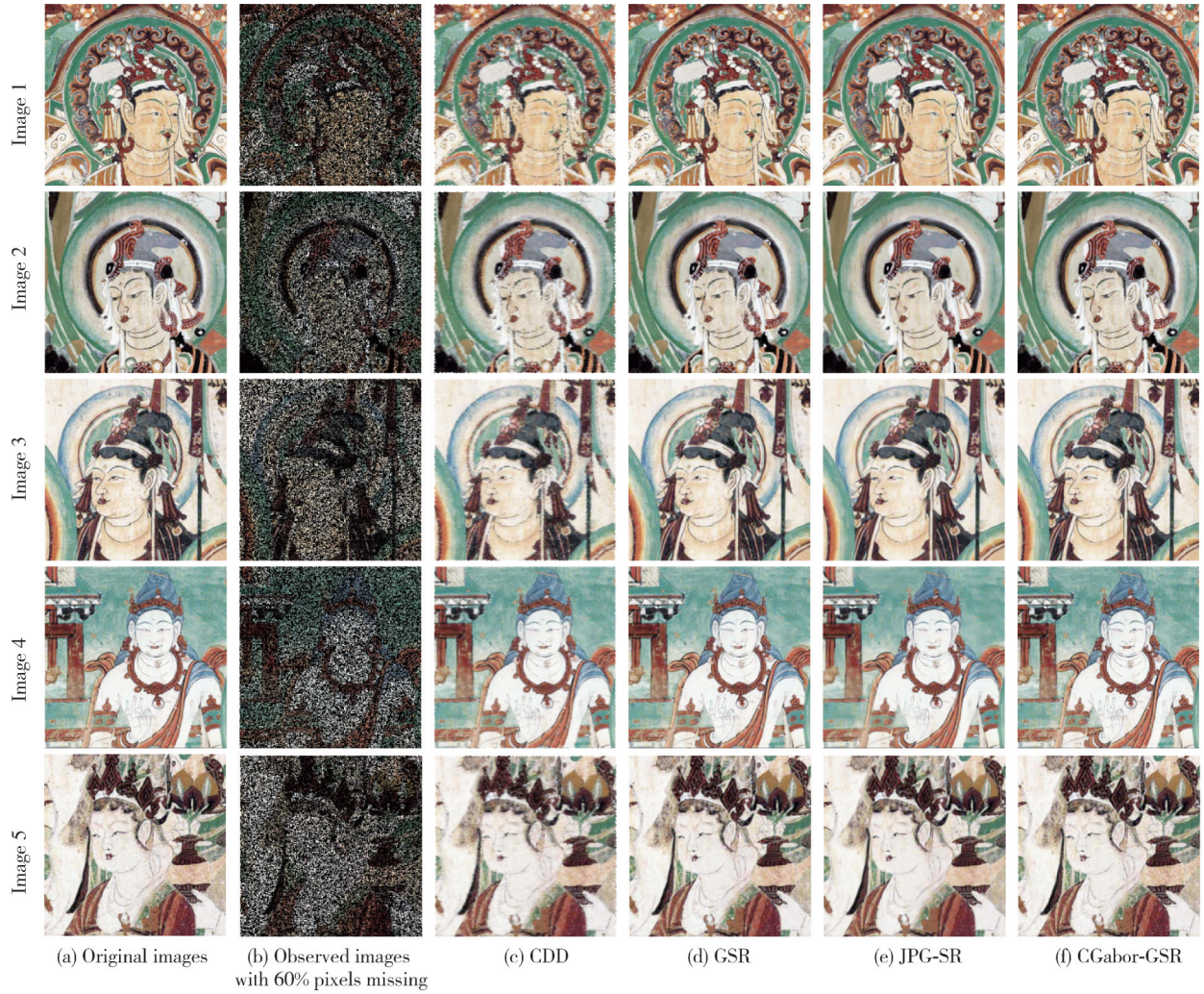

Fig. 5 Comparison of inpainting results of murals with randomly missing pixels

3.2 Artificially induced damaged images

The experiments of repairing the artificially induced damaged images were carried out by using CDD, GSR, JPG-SR, Criminisi[14], and CGabor-GSR, respectively, and the damaged images were obtained via the binary mask with artificial marker. The experimental results are shown in Fig. 6. Fig. 6(a) shows the original Dunhuang mural images, and Fig. 6(b) shows the damaged images. The inpainting results of CDD, Criminisi, GSR, JPG-SR and CGabor-GSR are presented in Fig. 6(c)—(g), respectively. It can be observed that the repair results of the CDD are incomplete, and this diffusion repair method has obvious repair residues at the scratches. Since the Criminisi algorithm based on matching sample blocks for repair does not take into account the structural information of the murals, it is determined only by the color Euclidean distance when selecting the matching block to repair it, followed by structure propagation errors and pixel errors matching phenomena, as shown in Fig. 6(d). Both GSR and JPG-SR produce incoherent lines and unclear structures, as shown in Fig. 6(e) and (f), where the lines within the rectangular frames are discontinuous and fuzzy. CGabor-GSR has better visual effects on the continuity and texture clarity of the damaged mural lines, which is more in line with the subjectively visual experience.

3.3 Really damaged mural images

To further verify the effectiveness of CGabor-GSR, four groups of really damaged mural images are used for repair experiments. The really damaged mural images are obtained with the binary masks generated according to the characteristics of the really damaged shapes. The experimental results are shown in Fig. 7, in which Fig. 7(a) is the real mural image and Fig. 7(b) is the mask image. Fig. 7(c) shows the repair results of CDD algorithm. From the rectangular boxes of the repair results of the first and fourth murals, it can be seen that the repair of the algorithm is not complete and the structure is fuzzy.

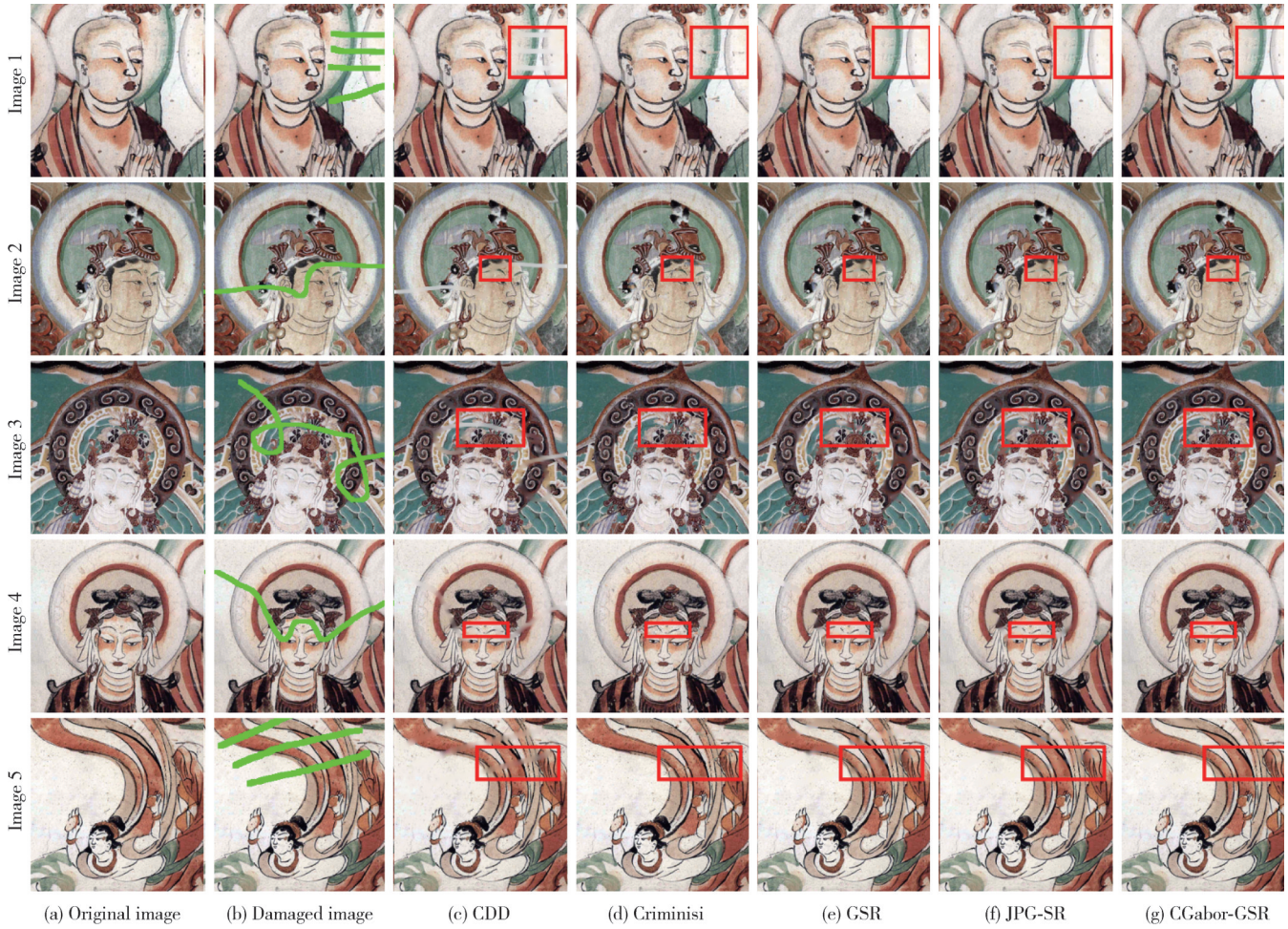

Fig. 6 Comparison of inpainting results of artificially damaged mural images

Fig.7 (d) shows the problem of pixel matching errors in the repair results of Criminisi algorithm, such as structure propagation error in the rectangular box of the repair result of the first mural, and block matching error in the fourth mural. Fig. 7 (e) shows the results of GSR restoration. From the rectangular box of the fourth mural, it can be found that there are obvious traces of restoration. Fig.7 (f) shows the results of JPG-SR restoration. From the rectangle boxes of the first mural and the third mural, it can be found that the restoration has not been complete. Fig.7 (g) is the results of CGabor-GSR. It can be seen that the restoration results have been improved in the continuity and clarity of lines.

In order to further quantitatively evaluate the repair results in Fig. 7, PSNR, SSIM and time are used for quantitative comparison and analysis.

Table 2 shows the PSNR and SSIM of the repair results in Fig. 5 by different algorithms. Table 3 is the repair time of different algorithms to the repair results in Fig.6.

Table 2 Comparison of PSNR and SSIM values of four algorithms when inpainting the images with randomly missing pixels

Image No.	CDD		Criminisi		GSR		JPG-SR		CGabor-GSR	
	PSNR /dB	SSIM	PSNR /dB	SSIM	PSNR /dB	SSIM	PSNR /dB	SSIM	PSNR /dB	SSIM
1	30.905 8	0.967 1	32.836 6	0.972 6	37.802 1	0.982 6	37.899 5	0.979 2	**38.946 5**	**0.986 1**
2	27.279 4	0.973 2	32.228 3	0.977 8	34.764 3	0.985 1	34.590 7	0.981 7	**39.688 7**	**0.992 1**
3	25.983 3	0.949 1	25.348 5	0.944 1	29.522	0.962 3	29.604 3	0.958 4	**37.867 8**	**0.989 9**
4	30.222 1	0.970 8	29.338 4	0.970 5	31.898 8	0.978 3	32.351 4	0.975 6	**39.082 9**	**0.990 1**
5	26.735 7	0.931 5	28.736 1	0.956 1	28.940 8	0.961 1	29.377 6	0.958 7	**37.548 1**	**0.981 7**

It can be found that the CGabor-GSR is superior to other comparison algorithms in terms of PSNR and SSIM. It can also be seen from Table 3 that although the CDD and Criminisi algorithm spend shorter repair time, the repair effect of CDD algorithm is poor and the damaged image cannot be completely repaired, and the Criminisi algorithm has pixel matching errors. The GSR and JPG-SR spend much longer repair time than CGabor-GSR. Comparatively, CGabor-GSR has high efficiency in case of good repair effect.

Fig. 7 Comparison of inpainting results of really damaged mural images

Table 3 Comparison of time values of four algorithms when inpainting damaged images

Image No.	Time/s				
	CDD	Criminisi	GSR	JPG-SR	CGabor-GSR
1	**4.492 1**	145.570 8	844.861 8	428.754 2	192.998 2
2	**2.742 2**	98.295 1	756.421 3	647.457 2	139.003 5
3	**3.225 9**	180.766 5	757.505 4	2 801.256 0	302.972 2
4	**2.975 5**	121.548 8	765.034 7	1 078.170 1	198.687 5
5	**4.478 1**	231.456 7	752.203 4	1 959.642 0	351.026 1

4 Conclusions

This paper presents the CGabor-GSR method to inpaint the Dunhuang murals. It has two significant merits: firstly, it uses mutual information to weight the Euclidean distance, overcoming the shortcomings of only relying on the color Euclidean distance for group division; secondly, it proposes the curvature Gabor wavelet transform to form multi-scale and multi-directional curvature feature information on the similar structure group, and then combines with PCA dimensionality reduction to get the initial structure group feature dictionary, avoiding the drawback of random selection of dictionary initialization. Experimental results have shown that CGabor-GSR model achieves significant performance improvements on the ancient mural image inpainting over compared algorithms in both objective values and visual evaluation. Although CGabor-GSR can produce good restoration results, it pays relatively less attention to the semantic factors of mural images. In the future, religious and cultural factors of ancient murals can be included, and deep learning methods can be applied for further research in mural restoration.

Acknowledgement

This work was supported by National Natural Science Foundation of China (No. 61963023), Humanities and Social Sciences Youth Foundation of Ministry of Education (No. 19YJC760012), and Lanzhou Jiaotong University Basic Top-Notch Personnel Project (No.2022JC36).

Declaration of conflicting interests

The authors have no conflict of interests related to this publication.

References

[1] ZHANG Y J, LIU T T, CATTANI C, et al. Diffusion-based image inpainting forensics *via* weighted least squares filtering enhancement. Multimedia Tools and Applications, 2021, 80(20): 30725-30739.

[2] RATHISH KUMAR B V, HALIM A. A linear fourth-order PDE-based gray-scale image inpainting model. Computational and Applied Mathematics, 2019, 38(1): 6.

[3] ABDULLA A A, AHMED M W. An improved image quality algorithm for exemplar-based image inpainting. Multimedia Tools and Applications, 2021, 80(9): 13143-13156.

[4] YANG S Y, LIANG H T, WANG Y, et al. Image inpainting based on multi-patch match with adaptive size. Applied Sciences, 2020, 10(14): 4921.

[5] WAN W, LIU J. Nonlocal patches based Gaussian mixture model for image inpainting. Applied Mathematical Modelling, 2020, 87: 317-331.

[6] LI Z D, CHENG J X, LIU J W. MRF image inpainting algorithm based on structure offsets statistics and multi-direction features. Acta Electronica Sinica, 2020, 48(5): 985-989.

[7] ZHAO D, DU H Q, MEI W B. Hybrid weighted l_1-total variation constrained reconstruction for MR image. Chinese Journal of Electronics, 2014, 23(4): 747-752.

[8] ZHANG L, KANG B S, LIU B T, et al. Image inpainting based on exemplar and sparse representation. International Journal of Signal Processing, Image Processing and Pattern Recognition, 2016, 9(9): 177-188.

[9] MO J C, ZHOU Y C. The research of image inpainting algorithm using self-adaptive group structure and sparse representation. Cluster Computing, 2019, 22(3): 7593-7601.

[10] WANG B, HU L L, CAO J J, et al. Image inpainting method based on sparse optimization in wavelet domain. Acta Electronica Sinica, 2016, 44(3): 600-606.

[11] BERTALMIO M, SAPIRO G, CASELLES V, et al. Image inpainting//The 27th Annual Conference on Computer Graphics and Interactive Techniques, July 1, 2000, New Orleans, LA, USA. New York: ACM Press, 2000: 417-424.

[12] SHEN J H, CHAN T F. Mathematical models for local nontexture inpaintings. SIAM Journal on Applied Mathematics, 2002, 62(3): 1019-1043.

[13] CHAN T F, SHEN J H. Nontexture inpainting by curvature-driven diffusions. Journal of Visual Communication and Image Representation, 2001, 12(4): 436-449.

[14] ZHANG L, KANG B, LIU B, et al. A new inpainting method for object removal based on patch local feature and sparse representation. International Journal of Innovative Computing Information and Control, 2016, 12(1): 113-124.

[15] WANG M H, YAN B, NGAN K N. An efficient framework for image/video inpainting. Image Communication, 2013, 28(7): 753-762.

[16] CRIMINISI A, PEREZ P, TOYAMA K. Region filling and object removal by exemplar-based image inpainting. IEEE Transactions on Image Processing, 2004, 13(9): 1200-1212.

[17] BITTENS S, PLONKA G. Real sparse fast DCT for vectors with short support. Linear Algebra and Its Applications, 2019, 582: 359-390.

[18] WANG H C, TAO C H, CHEN S C, et al. High-precision seismic data reconstruction with multi-domain

sparsity constraints based on curvelet and high-resolution Radon transforms. Journal of Applied Geophysics, 2019, 162: 128-137.
[19] AHARON M, ELAD M, BRUCKSTEIN A. K-SVD: an algorithm for designing overcomplete dictionaries for sparse representation. IEEE Transactions on Signal Processing, 2006, 54(11): 4311-4322.
[20] QIN Y. A new family of model-based impulsive wavelets and their sparse representation for rolling bearing fault diagnosis. IEEE Transactions on Industrial Electronics, 2018, 65(3): 2716-2726.
[21] ZHANG J, ZHAO D B, GAO W. Group-based sparse representation for image restoration. IEEE Transactions on Image Processing, 2014, 23(8): 3336-3351.
[22] ZHA Z Y, YUAN X, WEN B H, et al. Image restoration using joint patch-group-based sparse representation. IEEE Transactions on Image Processing, 2020, 29: 7735-7750.
[23] KONG Y F, ZHOU C Y, ZHANG C Y, et al. Multi-color channels based group sparse model for image restoration. Algorithms, 2022, 15(6): 176.
[24] WANG H, LI L, LI Q, et al. A mural inpainting method combining global consistency and local continuity. Journal of Hunan University (Natural Sciences). 2022, 49(6): 135-145.
[25] GUO K H, LABATE D, RODRIGUEZ AYLLON J P. Image inpainting using sparse multiscale representations: Image recovery performance guarantees. Applied and Computational Harmonic Analysis, 2020, 49(2): 343-380.
[26] DONOHO D L. For most large underdetermined systems of equations, the minimal 1-norm near-solution approximates the sparsest near-solution. Communications on Pure and Applied Mathematics, 2006, 59(7): 907-934.
[27] CANDES E J, TAO T. Decoding by linear programming. IEEE Transactions on Information Theory, 2005, 51(12): 4203-4215.
[28] DONG W S, ZHANG L, SHI G M, et al. Image deblurring and super-resolution by adaptive sparse domain selection and adaptive regularization. IEEE Transactions on Image Processing, 2011, 20(7): 1838-1857.
[29] LIAN Q S, SHI B S, CHEN S Z. Research advances on dictionary learning models, algorithms and applications. Acta Automatica Sinica, 2015, 41(2): 240-260.
[30] WEN Y, XU C, LU Y, et al. Gabor feature-based LogDemons with inertial constraint for nonrigid image registration. IEEE Transactions on Image Processing, 2020, 29: 8238-8250.
[31] LIU J, JING X J, SUN S L, et al. Local Gabor dominant direction pattern for face recognition. Chinese Journal of Electronics, 2015, 24(2): 245-250.
[32] LEE T S. Image representation using 2D Gabor wavelets. IEEE Transactions on Pattern Analysis and Machine Intelligence, 1996, 18(10): 959-971.
[33] GOLDSTEIN T, OSHER S. The split Bregman method for L1-regularized problems. SIAM Journal on Imaging Sciences, 2009, 2(2): 323-343.
[34] ZHANG J, ZHAO D B, XIONG R Q, et al. Image restoration using joint statistical modeling in a space-transform domain. IEEE Transactions on Circuits and Systems for Video Technology, 2014, 24(6): 915-928.
[35] HE B S, LIU H, WANG Z R, et al. A strictly contractive peaceman-rachford splitting method for convex programming. SIAM Journal on Optimization, 2014, 24(3): 1011-1040.

改进曲率Gabor变换和群稀疏表示的古壁画修复

赵梦雪[1], 陈　永[1,2*], 陶美凤[1]

1. 兰州交通大学 电子与信息工程学院, 甘肃 兰州 730070;
2. 甘肃省人工智能与图形图像处理工程研究中心, 甘肃 兰州 730070

摘　要： 稀疏表示在各种图像处理和计算机视觉任务中取得了极大的成功。在古壁画图像修复中，传统群稀疏表示模型仅通过欧几里得距离构造相似群并随机初始化字典，通常会导致结构模糊和线条不连续。为解决上述问题，提出了一种适用于敦煌古壁画修复的改进曲率Gabor变换和群稀疏表示（Curvature Gabor transform and group sparse representation，CGabor-GSR）模型。首先，引入互信息以加权欧几里得距离，并使用加权欧氏距离作为相似性群的新标准。其次，为避免字典初始化的随机性，提出一种曲率Gabor小波变换来提取特征，并通过主成分分析方法（Principal component analysis，PCA）降维初始化特征字典。最后，利用奇异值分解（Singular value decomposition，SVD）和分裂布雷格曼迭代（Split Bregman iteration，SBI））对模型进行重构，实现壁画图像重建。敦煌壁画修复的实验结果表明，该方法在客观评价和视觉评价方面均优于所比较算法。

关键词： 数字图像处理；壁画修复；曲率Gabor小波变换；群稀疏表示；互信息

引用格式： ZHAO Mengxue, CHEN Yong, TAO Meifeng. Improved Gabor transform and group sparse representation for ancient mural inpainting. Journal of Measurement Science and Instrumentation, 2025, 16(3): 384-394. DOI: 10.62756/jmsi. 1674-8042.2025037